

Influence of $\text{ZrO}_2\text{-Y}_2\text{O}_3$ and $\text{ZrO}_2\text{-CaO}$ coatings on microstructural and mechanical properties on Mg-1,3Ca-5,5Zr biodegradable alloy

B Istrate¹, C Munteanu¹, MN Matei², B Oprisan³, D Chicet⁴ and K Earar²

¹“Gheorghe Asachi” Technical University of Iasi, Faculty of Mechanical Engineering, 43 “D. Mangeron” Street, 700050, Iasi, Romania

²“Dunarea de Jos” University of Galati, Faculty of Medicine, Dental Medicine, Al. I. Cuza 35 Street, Galati, Romania

³“Gr.T. Popa” Medicine University of Iasi, Faculty of General Medicine, University street nr. 16, Iasi, Romania

⁴“Gheorghe Asachi” Technical University of Iasi, Faculty of Material Science and Engineering, 61-63 “D. Mangeron” Street, 700050, Iasi, Romania

E-mail: cornelmun@gmail.com

Abstract. Zirconia (ZrO_2) as a ceramic biomaterial facilitates the osteoconductivity in new bone formation around implant. In order to improve the degradation and the surface properties, it is necessary to apply a surface film to satisfy multiple clinical requirements such as mechanical strength, biocompatibility, and degradation rate. Therefore, surface changing to form a tenacious, biocompatible and corrosion resistant modified layer has become a necessary study in biodegradable materials. The aim of the study is to observe the morphology, structural and scratch analysis for some coatings of $\text{ZrO}_2\text{-CaO}$ and $\text{ZrO}_2\text{-Y}_2\text{O}_3$ having similar thickness deposited with an atmospheric plasma spraying facility, Sulzer Metco 9MCE, using scanning electron microscopy and X-Ray diffraction. Some mechanical aspects were highlighted during the scratch test. Comparative scratch tests were carried out to study the bonding properties between the coatings and the substrates.

1. Introduction

Mg and most of its alloy are considered to be relatively safe materials for human body. Pure Mg and Mg-X alloys (X:Ca, Si, Zn, Zr) seems attractive for medical use. Some impurities like: Fe, Ni, Cu in magnesium give low corrosion resistance. Qiao et al. [1] investigated that magnesium alloys with Fe concentration of 35 ppm accelerates the corrosion up to 60 times.

Ca belongs to second group of the periodic table. Calcium's solubility in magnesium is relatively low, about 1.34 wt.% under equilibrium conditions. Supersaturated Ca, 1.34 wt.% conducts to formation of Mg_2Ca compound along the grain boundaries. Alloying calcium in magnesium alloys helps refining the microstructure of Mg and gives mechanical strength and creep properties. Wan et al. [2] investigated that introducing 0.6 wt.% of Ca addition improves compressive strength of pure Mg.



Reviewing the corrosion behavior of the magnesium alloys, the most suitable calcium content should be between of 0.6–1.2 wt. % [3-5]. Gu et al. [5] estimated that 1-1.5 wt.% of Zr addition in magnesium alloys improves the tensile strength and materials ductility, having values of ultimate tensile strength of 171.87 MPa, elongation of 27.2%, and the corrosion rate is decreased by 40-50%. Zhou et al. [6] obtained the Mg–Ca–Zr alloys which higher values for tensile strength and elongation when zirconium concentration is between 0.5 wt. % to 1.2 wt. %. The as-cast Mg–1Ca–1Zr alloy reveals a value of 125 MPa for ultimate tensile strength and 8% in elongation to failure. [7]. A way to improve corrosion resistance on magnesium alloys is surface coatings. Piconi et al. [8] reveals that cytotoxicity of ZrO_2 is lower than TiO_2 . Bozzini et al. [9] demonstrated that ZrO_2 has a satisfactory biocompatibility and could be used as coating for biodegradable materials. Plasma spraying ZrO_2 layer is a ceramic coating used for corrosion resistance of metallic components [10, 11]. Li et al. [12] obtained a polylactic-co-glycolic acid (PLGA) coating on Mg6Zn alloy. He realized two coatings of 33 μm thickness, respectively 72 μm thicknesses. The 72 μm coating exhibits a lower corrosion resistance than the thinner coating. In vitro analysis with cell culture tests (MC3T3-E1) cells on coatings resulted good adhesion of cells on the PLGA coating. The purpose of this work was to obtain two ceramic coatings (ZrO_2 - Y_2O_3 / ZrO_2 -CaO) using atmospheric plasma spraying and to investigate the morphology, phase analysis and some mechanical characteristics.

2. Materials and methods

Mg-1.3Ca-5.5Zr alloy was obtained by melting in a induction current with controlled atmosphere facility, CTC50K15 type, using zirconia crucibles at Faculty of Materials Science and Engineering, University “Politehnica” of Bucharest, Laboratory of casting and refining metal alloys [13]. For casting it was used as raw materials pure magnesium (99.7%), pure calcium particles and a master Mg-25Zr alloy. Chemical composition correction was made by repeated casting until final composition of 1.3% Ca(wt.%) and 5.5% Zr(wt.%).

The chemical compositions has been determined by EDX analysis using a scanning electron microscope SEM Quanta 200 3D DUAL BEAM equipped with EDS-EDAX detector. The above mentioned percentages of alloying elements have been calculated as average of three values. Ceramic coatings of ZrO_2 - Y_2O_3 / ZrO_2 -CaO on Mg-Ca-Zr alloy were obtained using atmospheric plasma spray facility (SPRAYWIZARD-9MCE, Sultzer-Metco, USA). For phase analysis, XRD analysis was carried out using a X'Pert Pro MPD diffractometer. Apparent coefficient of friction, hardness and elastic modulus were measured using CETR UMT-2 Tribometer. For micro-scratch analysis it was used a constant load method with a load of 5N on a distance of 4 mm, for a single determination. In figure 1 is shown the EDS analysis and the chemical composition of the ceramic coatings on Mg-1,3Ca-5,5Zr alloy after deposition. In table 1 are highlighted the technological parameters used for the coating process.

Table 1. Technological parameters used for coating process.

| Powder | Gun | N ₂ | | H ₂ | | Electric | | Powder feeder 9MP | | | Spray distance (mm) |
|--|-----|----------------|-----------------|----------------|-----------------|----------|--------|-------------------------|--------------------|------------------|---------------------|
| | | Pressure (bar) | Gas flow (NLPM) | Pressure (bar) | Gas flow (NLPM) | DC (A) | DC (V) | Carrier gas flow (NLPM) | Air Pressure (bar) | Quantity (g/min) | |
| ZrO ₂ – CaO | 9MB | 3,4 | 44 | 3,4 | 6,6 | 400 | 70-80 | 5.3 | 1.4 | 144 | 127 |
| ZrO ₂ – Y ₂ O ₃ | | 3,6 | 39 | 3,4 | 6,6 | 400 | 70-80 | 5.1 | 1.4 | 126 | 127 |

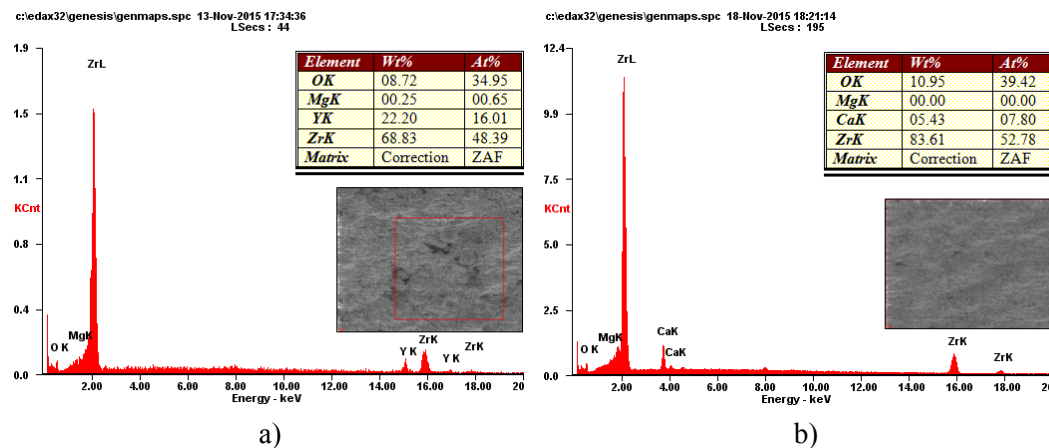


Figure 1. EDS spectrum and chemical composition of : a) ZrO₂-Y₂O₃; b) ZrO₂-CaO.

3. Results and discussions

3.1. Structural analysis

3.1. SEM microstructure

Morphology of the ceramic coatings is presented using SEM Quanta 200 3D images. In figure 2 and 3 are shown cross-section and surface images (a-d) for ZrO₂-Y₂O₃ / ZrO₂-CaO layers. Ceramic coatings have the appearance of columnar grains called "splats" having an average roughness with the presence of micropores and some unmelted particles from the thermal deposition process. ZrO₂-Y₂O₃ layer presented some cracks due the recovery process. Average thickness of coatings are presented in figure 2(a) and 3(a), 124.72 μ m for ZrO₂-Y₂O₃ coating, respectively 100.05 μ m for ZrO₂-CaO.

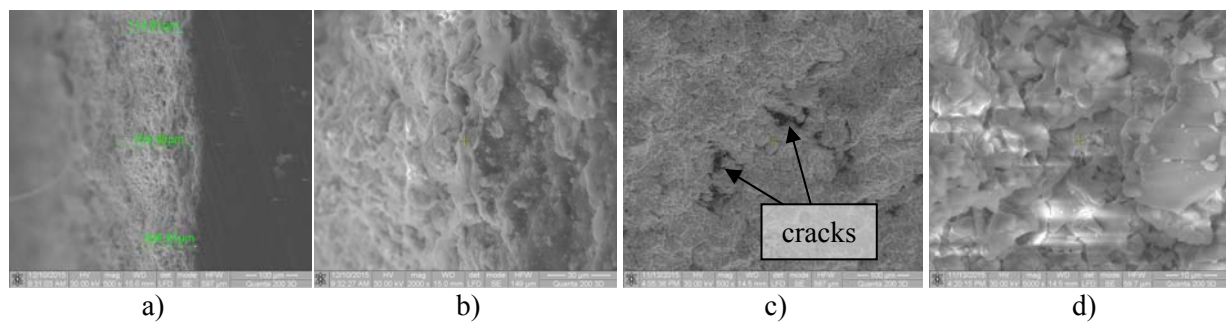


Figure 2. SEM images of ZrO₂-Y₂O₃ coating morphology: a) cross-section - 500X; b) cross-section - 2000X; c) surface - 500X; d) surface - 5000X.

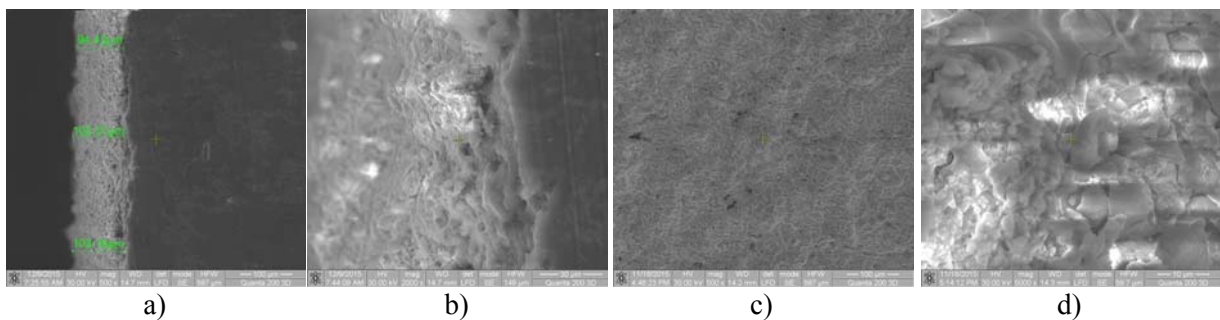


Figure 3. SEM images of ZrO₂-CaO coating morphology: a) cross-section - 500X; b) cross-section - 2000X; c) surface - 500X; d) surface - 5000X.

Studying the morphologies of the ceramic layers it can be noticed that $\text{ZrO}_2\text{-CaO}$ seems to be a more compact layer than $\text{ZrO}_2\text{-Y}_2\text{O}_3$ due the lack of micropores presented in the microstructure.

3.2. XRD analysis

XRD diffraction analysis are shown in figure 4. The diffraction analysis highlighted an $\alpha\text{-ZrO}_2$ predominant phase around 2θ angle: 30° and 50° having a tetragonal crystal system. Y_2O_3 compound is found most at 2θ angles: $73,47^\circ$, $94,27^\circ$ and $117,95^\circ$ with a crystal structure of cubic type. Calcium phase was identified at $2\theta = 73,92^\circ$ and $102,69^\circ$ with a cubic structure type. Lattice parameters of all identified compounds are shown in table 2.

Table 2. Lattice parameters of $\text{ZrO}_2\text{-Y}_2\text{O}_3$ / $\text{ZrO}_2\text{-CaO}$ coatings.

| | Compound | Space Group | Crystal system | a (Å) | b (Å) | c (Å) | α (°) | β (°) | γ (°) | Cell volume (10 ⁶ pm ³) |
|---|-------------------------------|-------------|----------------|---------|---------|---------|--------------|-------------|--------------|--|
| ZrO₂-Y₂O₃ coating | Mg | P63/mmc | Hexagonal | 3,2089 | 3,2089 | 5,2101 | 90 | 90 | 120 | 46,46 |
| | ZrO ₂ | P42/nmc | Tetragonal | 3,6292 | 3,6292 | 5,1973 | 90 | 90 | 90 | 68,45 |
| | ZrO ₂ | P42/nmc | Tetragonal | 3,6055 | 3,6055 | 5,1797 | 90 | 90 | 90 | 67,33 |
| | Y ₂ O ₃ | Ia-3 | Cubic | 10,6080 | 10,6080 | 10,6080 | 90 | 90 | 90 | 1193,70 |
| | YO _{1.335} | P-3m1E | Hexagonal | 3,8750 | 3,8750 | 6,0340 | 90 | 90 | 120 | 78,47 |
| ZrO₂-CaO coating | ZrO ₂ | Fm-3m | Cubic | 5,1280 | 5,1280 | 5,1280 | 90 | 90 | 90 | 134,85 |
| | ZrO ₂ | P42/nmc | Tetragonal | 3,5960 | 3,5960 | 5,1770 | 90 | 90 | 90 | 66,94 |
| | Ca | Fm-3m | Cubic | 5,5884 | 5,5884 | 5,5884 | 90 | 90 | 90 | 174,53 |
| | Ca | Fm-3m | Cubic | 5,5886 | 5,5886 | 5,5886 | 90 | 90 | 90 | 174,55 |

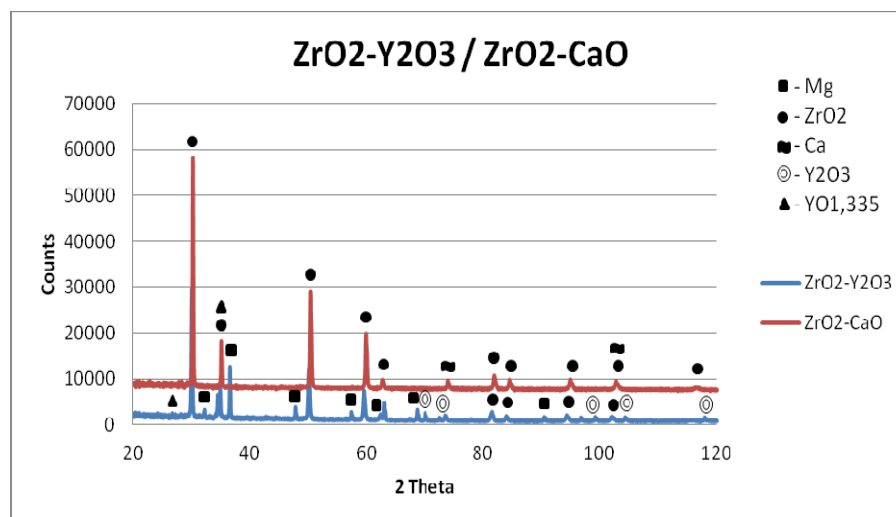


Figure 4. XRD patterns of $\text{ZrO}_2\text{-Y}_2\text{O}_3$ / $\text{ZrO}_2\text{-CaO}$ coatings.

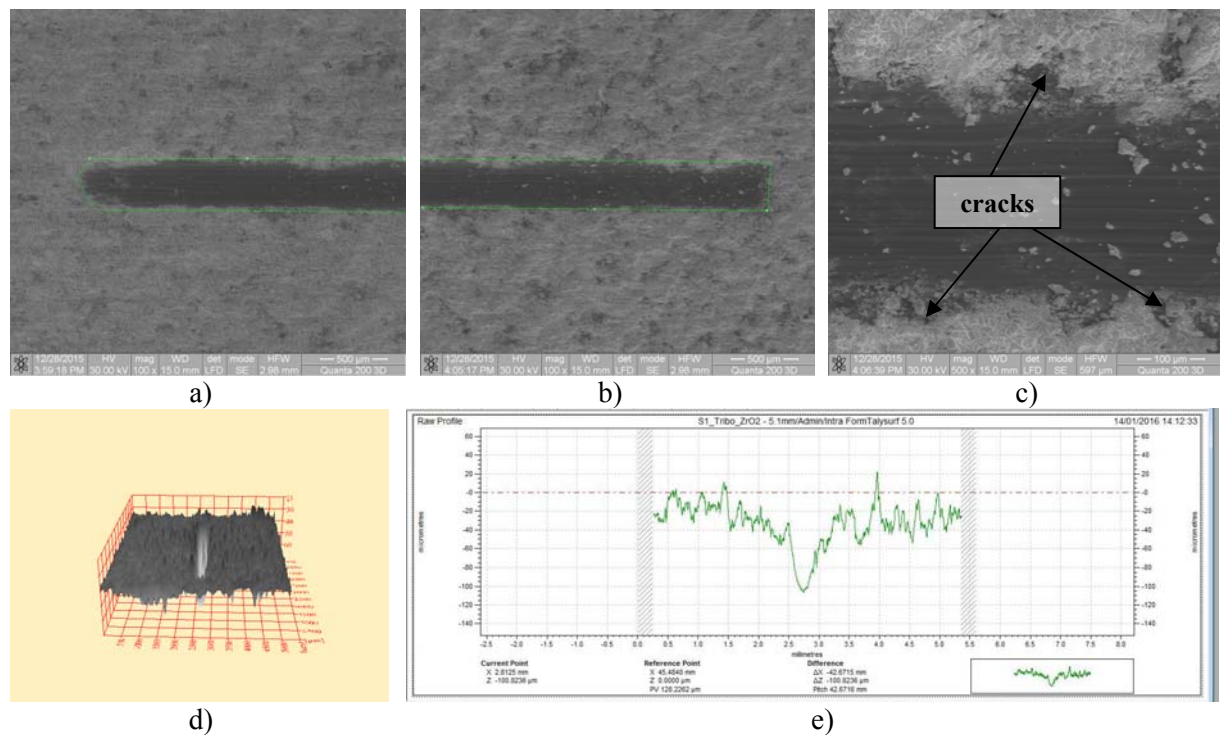
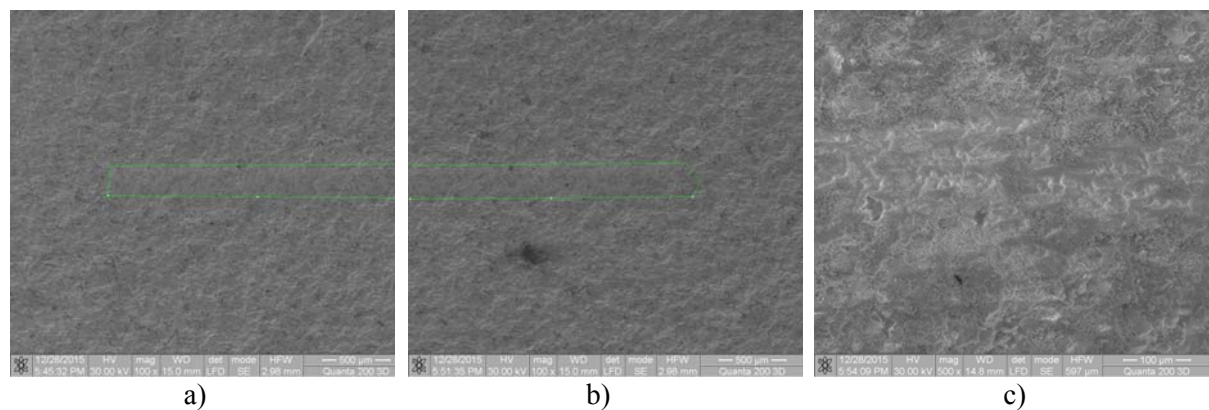
Using the the Scherrer equation [14], it was possible to calculate the crystallite size for each phase determinated and show the results in table 3.

Table 3. Crystalite size of compounds (nm).

| | ZrO ₂ | Y ₂ O ₃ | YO _{1,335} | ZrO ₂ | Ca |
|--|------------------|-------------------------------|---------------------|------------------|---------|
| ZrO ₂ – Y ₂ O ₃ | 23,94738 | 30,09688 | 24,79977 | - | - |
| ZrO ₂ – CaO | - | - | - | 22,4809 | 15,3444 |

3.3. Scratch and micro-indentation analysis

Figures 5 and 6 presents SEM images (a-c), 2-D (e) and 3-D (d) profile surface of the "scratch" analysis. Figure 5 a), b) is presented the head-ends of scratch marks, then a SEM image at 500X magnification, highlighting the fracturing of the ZrO₂-Y₂O₃ coating. The apparent coefficient of friction for the ZrO₂-Y₂O₃ layer is 0.868. Same analyses were carried out for the second layer, respectively ZrO₂-CaO, which presented an apparent coefficient of friction of 1.042.

**Figure 5.** SEM images of scratch test (a-c) and 2-D/3-D profile (d-e) on ZrO₂-Y₂O₃.

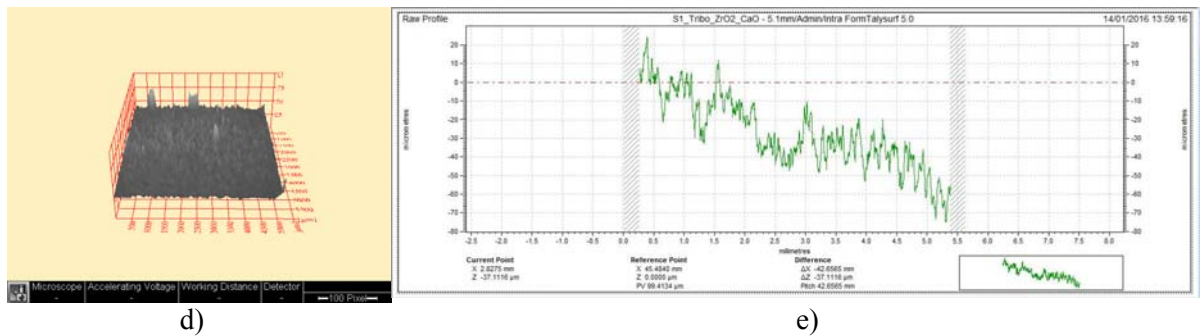


Figure 6. SEM images of scratch test (a-c) and 2-D/3-D profile (d-e) on $\text{ZrO}_2\text{-CaO}$.

SEM images showed an adherent layer (ZrO_2CaO) to the base material, a much harder coating (table 4) than $\text{ZrO}_2\text{-Y}_2\text{O}_3$ layer. Also it was noticed a lack of cracks in the layer of ZrO_2CaO , resulting a less fragile layer. The results have shown a depth of 65 microns for scratch of $\text{ZrO}_2\text{-Y}_2\text{O}_3$ layer with layer coated fracturing and 25 microns depth for scratch of $\text{ZrO}_2\text{-CaO}$ layer, without fracturing. it can be concluded that the layer of $\text{ZrO}_2\text{-CaO}$ has a high resistance to fracturing, a fact confirmed by hardness values and coefficient of friction apparently values presented in table 4.

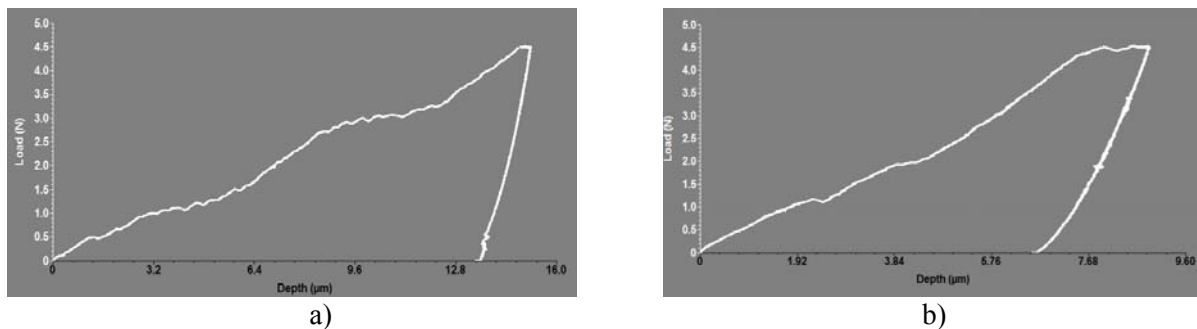


Figure 6. The variation curve of the micro-indentation test of $\text{ZrO}_2\text{-Y}_2\text{O}_3$ (a) / $\text{ZrO}_2\text{-CaO}$ (b) coatings.

$\text{ZrO}_2\text{-Y}_2\text{O}_3$ layer presented a strain load of approximately 14,6 μm and a strain release of approximately 13,2 μm resulting an elastic deformation of 1,4 μm . $\text{ZrO}_2\text{-CaO}$ layer showed a strain load of approximately 11,5 μm and a strain release of approximately 8,2 μm resulting an elastic deformation of 3,3 μm . These values indicate that $\text{ZrO}_2\text{-CaO}$ layer has an elastic behaviour towards $\text{ZrO}_2\text{-Y}_2\text{O}_3$ coating that is more fragile. Micro-indentation tests results are presented in table 4, showing the elastic modulus, hardness and stiffness for the ceramic layers.

Table 4. Some mechanical properties of $\text{ZrO}_2\text{-Y}_2\text{O}_3$ / $\text{ZrO}_2\text{-CaO}$ coatings.

| | COF | Hardness (HV) | Young Modulus (GPa) | Stiffness(N/ μm) |
|-------------------------------------|-------|---------------|---------------------|------------------------------|
| $\text{ZrO}_2\text{-Y}_2\text{O}_3$ | 0.868 | 20.053 | 20.541 | 3.733 |
| $\text{ZrO}_2\text{-CaO}$ | 1.042 | 41.229 | 17.903 | 2.377 |

4. Conclusions

In this article was studied the morphological appearance, X-ray diffraction, micro-scratch and micro-indentation aspects on ceramic coatings $\text{ZrO}_2\text{-Y}_2\text{O}_3$, respectively $\text{ZrO}_2\text{-CaO}$. These ceramic coatings have the appearance of columnar grains called "splats" having an average roughness with the presence of micropores and some unmelted particles from the thermal deposition process. X-Ray analysis showed the presence of $\alpha\text{-ZrO}_2$ as predominant phase having a tetragonal crystal system. Also was identified as secondary phase Y_2O_3 and calcium with a crystal structure of cubic type. $\text{ZrO}_2\text{-CaO}$

presented a higher fracturing resistance than ZrO₂-Y₂O₃, having a lower elastic modulus, with a higher hardness value. In conclusion ZrO₂-CaO coating behaved superior to mechanical tests than ZrO₂-Y₂O₃ coating which makes it suitable for further research in order to use in the medical field.

References

- [1] Qiao Z, Shi Z, Hort N, Zainal N, Abidin I and Atrens A 2012 Corrosion behavior of a nominally high purity Mg ingot produced by permanent mould direct chill casting *Corrosion Science* **61** pp 185–207
- [2] Wan Y, Xiong G, Luo H, He F, Huang Y and Zhou X 2008 Preparation and characterization of a new biomedical magnesium–calcium alloy *Materials & Design* **29** pp 2034–2037
- [3] Kim W C Kim J G Lee J Y and Seok H K 2008 Influence of Ca on the corrosion properties of magnesium for biomaterials *Materials Letters* **62** pp 4146–4148
- [4] Kirkland N T, Birbilis N, Walker J, Woodfield T, Dias G J and Staiger M P 2010 *Journal of Biomedical Materials Research Part B: Applied Biomaterials* **95B** pp 91–100
- [5] Gu X N, Zheng Y F, Cheng Y, Zhong S P and Xi T F 2009 In vitro corrosion and biocompatibility of binary magnesium alloys *Biomaterials* **30** pp 484–498
- [6] Zhou Y L, An J, Luo DM, Hu W Y, Li Y C, Hodgson P and Wen P C 2012 Microstructures and mechanical properties of as cast Mg–Zr–Ca alloys for biomedical applications *Materials Technology: Advanced Performance Materials* **27** pp 52–54
- [7] Zhang W, Li M, Chen Q, Hu W, Zhang W and Xin W 2012 Effects of Sr and Sn on microstructure and corrosion resistance of Mg–Zr–Ca magnesium alloy for biomedical applications *Materials & Design* **39** pp 379–383
- [8] Piconi C and Maccauro G 1999 Zirconia as a ceramic biomaterial-rev *Biomaterials* **20** 1-25
- [9] Bozzini B, Carlino P and Mele C 2011 Electrochemical behaviour and surface characterisation of Zr exposed to an SBF solution containing glycine, in view of dental implant applications, *Journal of Materials Science: Materials in Medicine* **22** pp 193-200
- [10] Morks M F, Gao Y, Fahim N F and Yingqing F U 2006 Microstructure and hardness properties of cermet coating sprayed by low power plasma *Materials Letters* **60** pp 1049-1053
- [11] Morks M F, Gao Y, Fahim N F, Yingqing F U and Shoeib M A 2005 Influence of binder materials on the properties of low power plasma sprayed cermet coatings *Surface & Coating Technology* **199** pp 66-71
- [12] Li J N, Cao P, Zhang X N, Zhang S X and He YH 2010 In vitro degradation and cell attachment of a PLGA coated biodegradable Mg–6Zn based alloy *Journal of Materials Science* **45(22)** pp 6038-6045
- [13] *** www.eramet.ro
- [14] Patterson A 1939 The Scherrer formula for X-ray particle size determination *Physical Review* **56** pp 978-982